JCTC Journal of Chemical Theory and Computation

Article

pubs.acs.org/JCTC

Accurate Coulomb Potentials for Periodic and Molecular Systems through Density Fitting

Mirko Franchini,[†,‡] Pierre Herman Theodoor Philipsen,[‡] Erik van Lenthe,[‡] and Lucas Visscher*[,†]

[†]Theoretical Chemistry, VU University Amsterdam, De Boelelaan 1083, NL-1081 HV Amsterdam, The Netherlands

[‡]Scientific Computing & Modelling NV, Theoretical Chemistry, VU University Amsterdam, De Boelelaan 1083, NL-1081 HV Amsterdam, The Netherlands

Supporting Information

ABSTRACT: We present a systematically improvable density fitting scheme designed for accurate Coulomb potential evaluation of periodic and molecular systems. The method does not depend on the way the density is calculated, allowing for a basis set expansion as well as a numerical representations of the orbitals. The scheme is characterized by a partitioning of the density into local contributions that are expanded by means of cubic splines. For three-dimensional periodic systems, the long-range contribution to the Coulomb potential is treated with the usual reciprocal space representation of the multipole moments, while in one- and two-dimensional systems, it is calculated via a new algorithm based on topological extrapolation. The efficiency and numerical robustness of the scheme is assessed for a number of periodic and nonperiodic systems within the framework of density-functional theory.

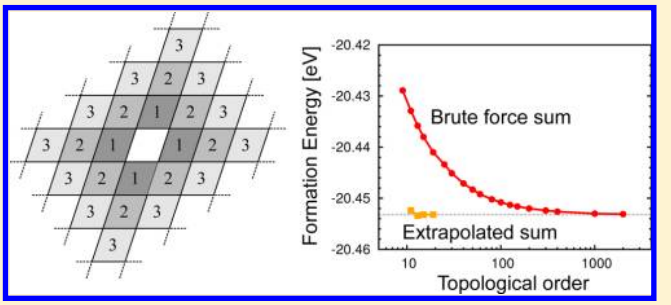

1. INTRODUCTION

One of the essential ingredients in Density-Functional Theory (DFT) is the Hartree energy, i.e., the classical Coulomb part of the electron−electron interaction. Implementations of DFT that use Slater Type Orbitals (STO) or Numerical Atomic Orbitals (NAO) as orbital expansion functions must rely on density fitting and numerical integration techniques because analytical integration is respectively unwieldy or impossible. But even when the Coulomb contributions can be readily evaluated analytically from the basis function representation of the electronic density, fitting techniques are often applied to enhance computational performance.[1] Also for calculation of the gradient and Hessian of the density, which are needed in the evaluation of the exchange-correlation (XC) part of the energy and potential, density fitting techniques are used to reduce the computational effort. In both cases, it is important to define an approximate representation of the electron density that can be systematically improved when a higher accuracy is desired. For application to the calculation of the Coulomb potential and interaction energy, an additional criterium is the ease with which these quantities can be computed. Depending on the nature of the system, different strategies are in use.

For 3D periodic systems, it is natural to build in the periodicity into the fit set. Plane wave expansions of the density are routinely used[2] for which an efficient evaluation of the Coulomb potential in reciprocal space can be achieved via Fourier transformations.[3] Extending this approach to systems with lower periodicity like slabs (2D), chains (1D), and molecules (0D) is possible by introducing an artificial 3D system. In this case, the resulting spurious interaction between the periodic images can be eliminated by either using dipole corrections[4] or modified Coulomb potentials.[5,6] Such corrections can be important when desired properties involve delocalized unoccupied electronic states.[7] Because of the uniform sampling of space by plane waves, the description of "empty" systems such as wide nanotubes, fullerenes, and metal−organic frameworks is somewhat less efficient than for dense systems.

For molecules, the most common approach for efficient evaluation of the Coulomb potential is to use an auxiliary fit set with predefined functions.[1,8−13] Expansion coefficients are obtained by minimizing (either globally or pairwise) the difference between the exact and fitted density for a particular metric. Although this class of fitting schemes has been successful in various applications, there are also some well-known problems. The set of fit functions in which the density is best expanded depends on the basis sets that is used, requiring updates of the fits sets when a new basis set becomes available. Furthermore, when employing spatially extended basis sets, the absolute accuracy is limited by overcompleteness and linear dependency problems. Because the fit sets are necessarily larger than the basis set itself, these problems are usually more severe for the fit set than for the primary basis set. The design of an optimal fit set is therefore of critical importance.[14] For functions that allow for analytical evaluation of Coulomb integrals, the procedure can be automatized by applying

Received: December 17, 2013

   dx.doi.org/10.1021/ct500172n | J. Chem. Theory Comput. XXXX, XXX, XXX−XXX

Cholesky decomposition techniques that determine the optimal fit set for a given target accuracy.[15]

The overcompleteness issue can be avoided by methods in which the density is expanded in strictly local numerical fit functions. The algorithm described in the present work belongs to this family of methods[16−20] and is related to the procedures proposed by Becke[16] and Delley.[17] In its current form, the method is not suitable for evaluation of the exchange integrals needed in hybrid DFT functionals. The scheme has been implemented in two DFT programs: the molecular STO-based program ADF[21] and the periodic NAO-based program BAND[12] (which can handle periodicity of any dimensionality, including molecules). We will show that this new efficient implementation significantly enhances the achievable accuracy.

The paper is organized as follows. In Section 2, we introduce the method for molecules, while in Section 3, we generalize to account for periodic systems. For such systems, the fitting itself is straightforward, but the evaluation of the Coulomb potential requires some attention. In Section 3.2, we describe a new topological extrapolation method that is suited for Coulomb potential evaluation in 1D and 2D systems. In Section 4, we define for the programs ADF and BAND four default settings ranging in quality from"default" to "excellent". In Section 5, we benchmark the method and these chosen defaults and discuss the computational scaling behavior.

2. DENSITY FITTING FOR MOLECULES

The quantity of interest is the Coulomb potential $V(\mathbf{r})$ of the system

$$V(\mathbf{r}) = \sum_{i=1}^{N_{\text{nuclei}}} \frac{Q_i}{|\mathbf{r} - \mathbf{R}_i|} + \int \frac{\rho(\mathbf{r}')}{|\mathbf{r} - \mathbf{r}'|} d\mathbf{r}' = V_{\text{nuclei}}(\mathbf{r}) + V_e(\mathbf{r}) \quad (1)$$

where $\rho(\mathbf{r})$ is the electronic density, and Q_i and $\mathbf{R}_i$, respectively, denote the charge and position of nucleus i. While the calculation of the nuclear potential $V_{\text{nuclei}}(\mathbf{r})$ is trivial, evaluation of the electronic potential $V_e(\mathbf{r})$ can be problematic. For STO or NAO basis functions, the integral in eq 1 has no simple analytical solution, and a direct numerical integration would be very expensive. We therefore first need to find an approximate density for which the integral in eq 1 can be evaluated efficiently. Our aim will be to use a set of systematically extendable numerical fit functions that allow for fast and accurate evaluation of the potential at any point in space.

2.1. Partitioning of the Density. Depending on the type of basis functions employed, the electron density in proximity of the nuclei may possess cusps at the nuclear positions and have a nontrivial radial behavior. Both aspects of the density are best handled in a spherical coordinates system centered on the corresponding nucleus. To be able to work in such a coordinate system, we first need to partition the density into local contributions that can be assigned to a nucleus

$$\rho(\mathbf{r}) = \sum_{i=1}^{N_{\text{nuclei}}} \rho_i(\mathbf{r}) \quad (2)$$

These contributions $\rho_i(\mathbf{r})$ should, apart from a possible cusp at the nucleus, be smooth functions with continuous derivatives. Such a partitioning can be achieved by means of a space partition function $p_i(\mathbf{r})$

$$\rho(\mathbf{r}) = \left(\sum_{i=1}^{N_{\text{nuclei}}} p_i(\mathbf{r})\right)\rho(\mathbf{r}) = \sum_{i=1}^{N_{\text{nuclei}}} \rho_i(\mathbf{r}) \quad (3)$$

where

$$\rho_i(\mathbf{r}) = p_i(\mathbf{r})\rho(\mathbf{r}) \quad (4)$$

For a given atom i, the smooth function $p_i(\mathbf{r})$ is 1 on the nucleus i and 0 on all other nuclei. A convenient definition is in terms of an unnormalized partition function $\mathcal{P}_i(\mathbf{r})$ as

$$p_i(\mathbf{r}) = \frac{\mathcal{P}_i(\mathbf{r})}{\sum_{j=1}^{N_{\text{nuclei}}} \mathcal{P}_j(\mathbf{r})} \quad (5)$$

Examples of suitable partition schemes can be found in the literature.[17,22−25] We employ the one described in our previous work, ref 26, which has been proven especially useful for periodic systems. $\mathcal{P}_i(\mathbf{r})$ is thereby defined as

$$\mathcal{P}_i(\mathbf{r}) = \eta_i \frac{e^{-2\|\mathbf{r}-\mathbf{R}_i\|/a_0}}{\|\mathbf{r} - \mathbf{R}_i\|^3} \quad (6)$$

where we introduce a size-adjustment parameter η_i chosen to be 0.3 $[a_0^3]$ for hydrogen and 1 $[a_0^3]$ for all other elements (a_0 denotes the Bohr radius). Thanks to the locality of $p_i(\mathbf{r})$, the resulting densities $\rho_i(\mathbf{r})$ are then strongly localized around the atom i. Furthermore, they are, apart from a possible cusp at the position $\mathbf{R}_i$, smooth functions over the whole space (including all other nuclear positions).

2.2. Expansion. With the partitioning into local contributions, each partial density $\rho_i(\mathbf{r})$ can be fitted separately in a polar coordinate system centered on the nucleus i ($\mathbf{r}_i$: $r_i\theta_i\phi_i = \mathbf{r} - \mathbf{R}_i$). The three-dimensional fitting problem is thereby decomposed in a finite series of two-dimensional polar expansions. To this aim, we create a radial grid for the interval $0 < r_i < +\infty$ by mapping a Gauss−Legendre quadrature grid for the finite interval $-1 < x < 1$ onto the interval $0 < r_i < +\infty$ via the mapping function

$$r(x) = \frac{\zeta}{\ln 2}(1 + x)\ln\frac{2}{1 - x} \quad (7)$$

where ζ is an atom-type dependent mapping parameter.[26,27] Employing such a numerical grid for the radial fitting ensures high flexibility and tunable monotonic convergency.

For each radial grid point p, we then need to fit the two-dimensional function $\overline{\rho}_{i,p}(\theta_i,\phi_i) := \rho_i(r_i = p,\theta_i,\phi_i)$. Real spherical harmonics (Z_{lm}) form a complete orthonormal basis set for the surface of a sphere and are therefore a natural choice as polar fit functions

$$\overline{\rho}_{i,p}(\theta_i,\phi_i) = \sum_{l=0}^{l_{\max}} \sum_{m=-l}^{l} c_{lm}^{ip} Z_{lm}(\theta_i,\phi_i) \quad (8)$$

Using the orthonormality of the spherical harmonics, the fit coefficients c_{lm}^{ip} are easily obtained by projection

$$c_{lm}^{ip} = \iint Z_{lm}(\theta_i,\phi_i)\overline{\rho}_{i,p}(\theta_i,\phi_i) d\theta_i d\phi_i \quad (9)$$

The polar integration in eq 9 is carried out numerically with octahedral Lebedev grids[28] (see Section 4 for details). The convergence of these expansions, a critical point for the efficiency of the scheme, will be discussed in Section 5. We would like to stress here that the above-mentioned "fitting grid" differs from the "integration grid" later to be used to evaluate

integrals, such as the elements of Fock matrix.[26] To be able to evaluate the fitted density in the integration grid, or any other point in space, we perform a spline interpolation[29] of the c_{lm}^{ip} coefficients with cubic spline functions $s_{lm}^{i}(r_i)$. Cubic splines are defined in the interval j between two adjacent grid points p, as

$$s_j(r) = a_j + b_j r + c_j r^2 + d_j r^3 \tag{10}$$

Cubic splines have continuous first and second derivatives. This is essential if the fitted density and its first and second derivatives are used, as in our implementation, in the computation of a generalized gradient approximation (GGA) exchange-correlation (XC) potential.

With this interpolation, the partitioned densities $\rho_i(\mathbf{r})$ are thus expressed as

$$\rho_i(\mathbf{r}) \approx \sum_{lm} Z_{lm}(\theta_i,\phi_i) s_{lm}^{i}(r_i) \tag{11}$$

and the total density is written as

$$\rho(\mathbf{r}) = \sum_{i=1}^{N_{\text{nuclei}}} \rho_i(\mathbf{r}) \approx \sum_{i=1}^{N_{\text{nuclei}}} \sum_{lm} Z_{lm}(\theta_i,\phi_i) s_{lm}^{i}(r_i) \tag{12}$$

In the limit of angular expansion up to $l = \infty$, perfect polar numerical integration and an infinitely fine radial grid, the expansion in eq 12 becomes exact. This feature allows for systematic testing of the numerical accuracy of the fit procedure and application-specific tuning of the accuracy.

2.3. Coulomb Potential Evaluation. Using the expansion of eq 12, the integral in eq 1 becomes

$$\begin{aligned} V_e(\mathbf{r}) &= \sum_{i=1}^{N_{\text{nuclei}}} \int \frac{\rho_i(\mathbf{r}')}{|\mathbf{r} - \mathbf{r}'|} \mathrm{d}\mathbf{r}' \\ &\approx \sum_{i=1}^{N_{\text{nuclei}}} \sum_{lm} \int \frac{Z_{lm}(\theta_i',\phi_i') s_{lm}^{i}(r_i')}{|\mathbf{r}_i - \mathbf{r}_i'|} \mathrm{d}\mathbf{r}_i' \end{aligned} \tag{13}$$

after which the Coulomb potential can be expanded in spherical harmonics[30] to obtain the desired analytical expression

$$V_e(\mathbf{r}) \approx \sum_{i=1}^{N_{\text{nuclei}}} \sum_{lm} \frac{4\pi}{2l+1} Z_{lm}(\theta_i,\phi_i) I_{lm}^{i}(r_i) \tag{14}$$

with $I_{lm}^{i}(r_i)$ being the one-dimensional integral

$$I_{lm}^{i}(r_i) = \frac{1}{r_i^{l+1}} \int_0^{r_i} r'^{l+2} s_{lm}^{i}(r') \mathrm{d}r' + r_i^{l} \int_{r_i}^{\infty} \frac{s_{lm}^{i}(r')}{r'^{l-1}} \mathrm{d}r' \tag{15}$$

The evaluation of the Coulomb potential in an arbitrary point r_i in the integration grid requires the evaluation of $I_{lm}^{i}(r_i)$ for which simple analytical expressions can be used because the spline functions $s_{lm}^{i}(r)$ are piecewise polynomials. Nonetheless, because a large number of integrals $I_{lm}^{i}(r_i)$ are needed, their evaluation can still be computationally demanding. To further improve efficiency of the scheme, the integrals $I_{lm}^{i}(r_i)$ are therefore calculated only in the radial grid points p on the fitting grid, and the resulting values are again interpolated by a cubic spline function $v_{lm}^{i}(r_i)$ to get the desired values on the integration grid. This double interpolation enhances significantly the performance of the potential evaluation and makes it possible to reach near-linear scaling. The total potential is finally written as

$$V_e(\mathbf{r}) \approx \sum_{i=1}^{N_{\text{nuclei}}} \sum_{lm} \frac{4\pi}{2l+1} Z_{lm}(\theta_i,\phi_i) v_{lm}^{i}(r_i) \tag{16}$$

2.4. Multipole Expansions at Large Distance. As a result of the local nature of the partition functions $p_i(\mathbf{r})$, each density $\rho_i(\mathbf{r})$ is strongly localized in space around the corresponding atom i. For each density $\rho_i(\mathbf{r})$, it is therefore possible to define a distance $r_i^{\max}$ (from the nucleus i) beyond which the density $\rho_i(\mathbf{r})$ can safely be considered negligible. For distances beyond this threshold, $r > r_i^{\max}$, the second term in eq 15 vanishes, resulting in the well-known multipole expression

$$V_e^{i}(\mathbf{r}) = \sum_{lm} \frac{4\pi}{2l+1} Z_{lm}(\theta_i,\phi_i) \frac{q_i^{l,m}}{r_i^{l+1}} \quad \text{if } r_i > r_i^{\max} \tag{17}$$

where $q_i^{l,m}$ are the atomic multipole moments

$$q_i^{l,m} = \int_0^{r_i^{\max}} s_{lm}^{i}(r') r'^{l+2} \mathrm{d}r' \tag{18}$$

The monopoles $q_i^{0,0}$ represent the charge allocated to atom i. In this work, these local charges serve just technical purposes; the precise amount of density allocated to an atomic center depends on the value chosen for the partitioning parameter η_i (see Section 2.1), which should be revised if the charges are to be used for interpretative purposes.

3. DENSITY FITTING IN PERIODIC SYSTEMS

For periodic systems, the fitting itself is straightforward as will be explained in Section 3.1. However, the extension of eq 1 for the Coulomb potential requires some care because the electronic and nuclear terms are diverging when summed individually over the infinitely many cells in an infinite crystal. This is a well-known consequence of the unphysical nature of an infinite periodic systems.[3] Rather than simply introducing a summation over all cells $\mathbf{R}$

$$V(\mathbf{r}) = \sum_{\mathbf{R}} V_{\text{n}}^{\text{cell}}(\mathbf{r} - \mathbf{R}) + \sum_{\mathbf{R}} V_{\text{e}}^{\text{cell}}(\mathbf{r} - \mathbf{R}) \tag{19}$$

(where $V_{\text{n}}^{\text{cell}}(\mathbf{r})$ and $V_{\text{e}}^{\text{cell}}(\mathbf{r})$ denote the nuclear and electronic potentials arising from an arbitrary central cell), we need to express the total electrostatic potential in terms of contributions from electrically neutral objects. To that end, we add and subtract to eq 19 the potential originating from a periodic reference density $\rho_{\text{atoms}}(\mathbf{r})$ consisting of a superposition of spherical atomic densities

$$\begin{aligned} V(\mathbf{r}) = \sum_{\mathbf{R}} \Bigg(&\sum_{i=1}^{N_{\text{nuclei}}} \frac{Q_i}{|\mathbf{r} - \mathbf{R} - \mathbf{R}_i|} + \int_{\text{cell}} \frac{\rho(\mathbf{r}')}{|\mathbf{r} - \mathbf{R} - \mathbf{r}'|} \mathrm{d}\mathbf{r}' \\ &+ \int_{\text{cell}} \frac{\rho_{\text{atoms}}(\mathbf{r}')}{|\mathbf{r} - \mathbf{R} - \mathbf{r}'|} \mathrm{d}\mathbf{r}' - \int_{\text{cell}} \frac{\rho_{\text{atoms}}(\mathbf{r}')}{|\mathbf{r} - \mathbf{R} - \mathbf{r}'|} \mathrm{d}\mathbf{r}' \Bigg) \end{aligned} \tag{20}$$

We can then define $V_{\text{ref}}(\mathbf{r})$ and $V_{\text{def}}(\mathbf{r})$ as

dx.doi.org/10.1021/ct500172n | J. Chem. Theory Comput. XXXX, XXX, XXX−XXX

$$V_{\mathrm{ref}}(\mathbf{r}) = \sum_{\mathbf{R}}\left(\sum_{i=1}^{N_{\mathrm{nuclei}}}\frac{Q_i}{|\mathbf{r}-\mathbf{R}-\mathbf{R}_i|} + \int_{\mathrm{cell}}\frac{\rho_{\mathrm{atoms}}(\mathbf{r}')}{|\mathbf{r}-\mathbf{R}-\mathbf{r}'|}\mathrm{d}\mathbf{r}'\right) = \sum_{\mathbf{R}} V_{\mathrm{ref}}^{\mathrm{cell}}(\mathbf{r}-\mathbf{R}) \tag{21}$$

and

$$V_{\mathrm{def}}(\mathbf{r}) = \sum_{\mathbf{R}}\left(\int_{\mathrm{cell}}\frac{\rho_{\mathrm{def}}(\mathbf{r}')}{|\mathbf{r}-\mathbf{R}-\mathbf{r}'|}\mathrm{d}\mathbf{r}'\right) = \sum_{\mathbf{R}} V_{\mathrm{def}}^{\mathrm{cell}}(\mathbf{r}-\mathbf{R}) \tag{22}$$

where we introduced the deformation density[12] $\rho_{\mathrm{def}}(\mathbf{r})$

$$\rho_{\mathrm{def}}(\mathbf{r}) = \rho(\mathbf{r}) - \rho_{\mathrm{atoms}}(\mathbf{r}) \tag{23}$$

Equation 19 becomes

$$V(\mathbf{r}) = V_{\mathrm{ref}}(\mathbf{r}) + V_{\mathrm{def}}(\mathbf{r}) \tag{24}$$

The potential $V_{\mathrm{ref}}^{\mathrm{cell}}$ (eq 21) has a vanishing monopole moment, and because it originates from a linear combination of spherical functions centered on the atoms, it can be easily evaluated.[12] The potential $V_{\mathrm{def}}^{\mathrm{cell}}$ (eq 22) arising from the deformation density ρ_{def} represents the "difficult" part of the problem at hand. Because the deformation density also has a vanishing monopole moment over the unit cell, the infinite summation over the lattice vectors in eq 22 is convergent, and the fitting scheme described in Section 2 can be adapted to evaluate its Coulomb integral.

3.1. Partition Function for Periodic Systems. In analogy with eq 3, the periodic deformation density ρ_{def} is partitioned into atomic contributions in the following fashion

$$\rho_{\mathrm{def}}(\mathbf{r}) = \left(\sum_{\mathbf{R}}\sum_{i=1}^{N_{\mathrm{nuclei}}} p_{i,\mathbf{R}}(\mathbf{r})\right)\rho_{\mathrm{def}}(\mathbf{r}) = \sum_{\mathbf{R}}\sum_{i=1}^{N_{\mathrm{nuclei}}}\rho_{i,\mathbf{R}}(\mathbf{r}) \tag{25}$$

where $\rho_{i,\mathbf{R}}(\mathbf{r}) = p_{i,\mathbf{R}}(\mathbf{r})\rho_{\mathrm{def}}(\mathbf{r})$. The partition function $p_{i,\mathbf{R}}(\mathbf{r})$, the periodic equivalent of eq 5, is defined as

$$p_{i,\mathbf{R}}(\mathbf{r}) = \frac{\mathcal{P}_{i,\mathbf{R}}(\mathbf{r})}{\sum_{\mathbf{R}'}\sum_{j=1}^{N_{\mathrm{nuclei}}}\mathcal{P}_{j,\mathbf{R}'}(\mathbf{r})} \tag{26}$$

the unnormalized partition function $\mathcal{P}_{i,U}(\mathbf{r})$ being[26]

$$\mathcal{P}_{i,\mathbf{R}}(\mathbf{r}) = \eta_i\frac{e^{-2\|\mathbf{r}-\mathbf{R}-\mathbf{R}_i\|/a_0}}{\|\mathbf{r}-\mathbf{R}-\mathbf{R}_i\|^3} \tag{27}$$

Although no longer periodic, the partitioned densities $\rho_{i,\mathbf{R}}(\mathbf{r})$ are related by simple lattice vector translations

$$\rho_{i,\mathbf{R}}(\mathbf{r}) = \rho_{i,\mathbf{R}'}(\mathbf{r}-\mathbf{R}+\mathbf{R}') \tag{28}$$

With this density partitioning into atom-centered contributions $\rho_{i,\mathbf{R}}(\mathbf{r})$, the expansion procedure is identical to the one described in Section 2.2, and the integral in eq 22 can be rewritten as

$$V_{\mathrm{def}}^{\mathrm{cell}}(\mathbf{r}) = \sum_{i=1}^{N_{\mathrm{nuclei}}}\int\frac{\rho_{i,0}(\mathbf{r}')}{|\mathbf{r}-\mathbf{r}'|}\mathrm{d}\mathbf{r}' \tag{29}$$

where the integration is now over the whole space rather than over the unit cell, and we use the subscript "0" to label the central unit cell.

3.2. Long-Range Coulomb Potential in Periodic Systems. Due to the extremely long-range nature of the electrostatic forces, the evaluation of the Coulomb potential in periodic systems needs careful consideration. The starting point is a real space sum over the (infinitely many) unit cells

$$V_{\mathrm{def}}(\mathbf{r}) = \sum_{\mathbf{R}} V_{\mathrm{def}}^{\mathrm{cell}}(\mathbf{r}-\mathbf{R}) \tag{30}$$

with

$$V_{\mathrm{def}}^{\mathrm{cell}}(\mathbf{r}) = \sum_{i=1}^{N_{\mathrm{nuclei}}}\begin{cases}\sum_{lm}\frac{4\pi}{2l+1}Z_{lm}(\theta_i,\phi_i)v_{lm}^{i}(r_i) & \text{if } r_i \le r_i^{\max}\\ \sum_{lm}\frac{4\pi}{2l+1}Z_{lm}(\theta_i,\phi_i)\frac{q_i^{l,m}}{r_i^{l+1}} & \text{if } r_i > r_i^{\max}\end{cases} \tag{31}$$

A direct lattice summation of the Coulomb potential in 3D systems (apart from being computationally inconvenient) leads to a conditionally converging sum, the result depending on the order in which the cell summation is carried out.[13,31,32] This seemingly unphysical result arises due to the fact that we are dealing with a fictitious system: an infinite crystal. Any partial sum (corresponding to a "real" finite crystal) should be independent of the summation order. Techniques to avoid direct lattice summations in infinite crystals can be found in textbooks[3] and generally exploit three-dimensional Fourier transforms, the Ewald summations being a notable example.[32] The incorporation of these standard techniques into the our fitting scheme is briefly sketched in Section 3.2.1.

For two- and one-dimensional systems, i.e., slabs and chains, the problem is far less explored, but direct lattice summations of the Coulomb potential are still computationally impractical due to their extremely slow convergence. The most common approaches for 1D and 2D systems are fast multipole moments schemes,[33,34] screening functions,[12] and reformulations of the 3D Ewald method with artificial three-dimensional repetitions of the lower-dimensional system.[35] Although these schemes are all feasible, we propose an alternative approach to approximate the long-range contribution of the Coulomb potential for 1D and 2D systems. The scheme, which will be described in detail in Sections 3.2.2 and 3.2.3, uses extrapolation of the Coulomb potential based on the exact contributions calculated for a finite (ideally small) number of nearby cells.

3.2.1. Three-Dimensional Periodic Systems. For three-dimensional systems, the long-range contribution to the Coulomb potential is best treated in reciprocal space. To this end, we add and subtract for each atom a combination of Gaussian densities with matching multipole moments

$$\rho_{\mathrm{def}}(\mathbf{r}) = (\rho_{\mathrm{def}}(\mathbf{r}) - \rho_{\mathrm{gauss}}(\mathbf{r})) + \rho_{\mathrm{gauss}}(\mathbf{r}) \tag{32}$$

$$\rho_{\mathrm{gauss}}(\mathbf{r}) = \sum_{\mathbf{R}}\sum_{i=1}^{N_{\mathrm{nuclei}}}\sum_{l=0}^{l_{\max}}\sum_{m=-l}^{l} -\frac{2l+1}{2\pi}\frac{q_i^{l,m}}{\gamma\left(\frac{l+3}{2}\right)\sigma^{l+3}} \times e^{-r_i^2/\sigma^2}Z_{lm}(\theta_i,\phi_i) \tag{33}$$

dx.doi.org/10.1021/ct500172n | J. Chem. Theory Comput. XXXX, XXX, XXX−XXX

where q_i^{lm} is the atomic multipole moments (eq 18), γ is the gamma function, and σ represents the width of the Gaussians, a constant of our choice.

The term $(\rho_{\text{def}}(\mathbf{r}) - \rho_{\text{gauss}}(\mathbf{r}))$ has vanishing multipole moments, and its extremely short-ranged potential can be evaluated via an explicit summation. The potential originating from the second term of eq 32 $(\rho_{\text{gauss}}(\mathbf{r}))$ is treated in reciprocal space.

$$V(\mathbf{r}) = \sum_{\mathrm{G}\neq 0} V_{\mathrm{G}} e^{i\mathrm{G}\mathbf{r}} \tag{34}$$

$$V_{\mathrm{G}} = \frac{4\pi}{\mathrm{G}^2}\rho_{\mathrm{G}} \quad \text{if } \mathrm{G} \neq 0 \tag{35}$$

$$\rho_{\mathrm{G}} = \frac{1}{v_{\text{cell}}}\int_{\text{cell}} \rho_{\text{gauss}}(\mathbf{r}) e^{-i\mathrm{G}\mathbf{r}} \tag{36}$$

were $\mathbf{G}$ represent the reciprocal lattice vectors, and v_{cell} is the volume of the unit cell. We note that discarding the $\mathbf{G} = 0$ component of the Coulomb potential in eq 34 is merely a convenient choice of gauge, with no effect on physical properties. This standard scheme has now been implemented in the BAND program for 3D-periodic systems.

3.2.2. Long-Range Potential Extrapolation for One-Dimensional Periodic Systems. We next turn to lower dimensional cases, starting with systems periodic in only one dimension, i.e., chains. In this case, the lattice vectors can be defined as $\mathbf{R} = na\mathbf{i}$, where n is an integer number, a is the cell size, and $\mathbf{i}$ represents a unit vector in the periodic direction (taken here as the x-axis).

We first consider the Coulomb potential contribution from cells at large distances from the central one. Let $\mathbf{r}$ be a point located in the central cell. Far from $\mathbf{r}$, the Coulomb potential originating from a cell $V_{\text{def}}^{\text{cell}}(\mathbf{r})$ reduces to a multipole expansion[30] for which the moments can be readily obtained by combining[36] the atomic multipole moments defined in Section 2.4. While individual atomic monopoles are in general nonzero, the monopole q_0 of a complete cell vanishes by construction (the integral of the deformation density over the unit cell is zero). The next terms in the expansion are the three components of the dipole moment vector $\mathbf{d}$ of the unit cell. The slowest decaying term arises from d_x and decays as $1/R^2$, while the potential originating from the orthogonal components d_y and d_z decay as $1/R^3$. Potentials associated with higher multipoles also decay as $1/R^3$ or faster.

Keeping this in mind, we can consider the full one-dimensional chain. We need to sum over all cells but can combine contributions from two opposite cells $-n$ and n that have an equal neighboring order $|n|$, which we call the topological distance. We thus write eq 30 as

$$\begin{aligned} V_{\text{def}}(\mathbf{r}) &= V_{\text{def}}^{\text{cell}}(\mathbf{r}) + \sum_{t=1}^{\infty}\left(V_{\text{def}}^{\text{cell}}(\mathbf{r} - ta\mathbf{i}) + V_{\text{def}}^{\text{cell}}(\mathbf{r} + ta\mathbf{i})\right) \\ &= V_{\text{def}}^{\text{cell}}(\mathbf{r}) + \sum_{t=1}^{\infty} V_t(\mathbf{r}) \end{aligned} \tag{37}$$

where

$$V_t(\mathbf{r}) = V_{\text{def}}^{\text{cell}}(\mathbf{r} - ta\mathbf{i}) + V_{\text{def}}^{\text{cell}}(\mathbf{r} + ta\mathbf{i}) \tag{38}$$

with the positive index t labeling the topological sets of cells. By isolating the dominant term, we may write eq 38 as

$$V_t(\mathbf{r}) \propto \frac{(x - ta)d_x}{\|\mathbf{r} - ta\mathbf{i}\|^3} + O\left(\frac{1}{\|\mathbf{r} - ta\mathbf{i}\|^3}\right) + \frac{(x + ta)d_x}{\|\mathbf{r} + ta\mathbf{i}\|^3} + O\left(\frac{1}{\|\mathbf{r} + ta\mathbf{i}\|^3}\right) \tag{39}$$

and consider its large distance limit. In this limit, the denominator becomes

$$\frac{1}{\|\mathbf{r} \pm ta\mathbf{i}\|^3} = \frac{1}{(ta)^3} + O\left(\frac{1}{t^4}\right) \text{ as } t \to \infty \tag{40}$$

and eq 39 simplifies to

$$V_{t\to\infty}(\mathbf{r}) \propto \frac{2xd_x}{(ta)^3} + O\left(\frac{1}{t^3}\right) = O\left(\frac{1}{t^3}\right) \tag{41}$$

We see that by grouping together the contributions from opposite cells, we eliminated the $O(1/t^2)$ contribution for large t. Equation 41 can be rewritten as

$$V_{t\to\infty}(\mathbf{r}) = \frac{c_3(\mathbf{r})}{t^3} + \frac{c_4(\mathbf{r})}{t^4} + \ldots \tag{42}$$

where the $c_i(\mathbf{r})$ coefficients are related to the cell's multipole moments. For large t, the expansion in eq 42 can further be safely truncated to a maximum order $i_{\max}$.

Although in a simple case it is in principle possible to evaluate the coefficients $c_i(\mathbf{r})$ from the cell's multipole moments, we pursue a different approach. We first evaluate $V_t(\mathbf{r})$ for a finite set of t values $(1 \le t \le t_{\text{fin}})$ using eq 31. We then take a subset $t_{\text{init}} \le t \le t_{\text{fin}}$ for which the asymptotic functional form of $V_t(\mathbf{r})$ shown in eq 42 represents a good approximation (this can be achieved by choosing t_{init} sufficiently large). The coefficients $c_i(\mathbf{r})$ can be obtained from a least-squares fit to the known values of $V_t(\mathbf{r})$ versus t and used to calculate the remaining contribution to the Coulomb potential

$$\begin{aligned} V_{\text{def}}(\mathbf{r}) &\approx V_{\text{def}}^{\text{cell}}(\mathbf{r}) + \sum_{t=1}^{t_{\text{fin}}} V_t(\mathbf{r}) + \sum_{t=t_{\text{fin}}+1}^{\infty}\sum_{i=3}^{i_{\max}} \frac{c_i(\mathbf{r})}{t^i} \\ &\approx V_{\text{def}}^{\text{cell}}(\mathbf{r}) + \sum_{t=1}^{t_{\text{fin}}} V_t(\mathbf{r}) + \sum_{i=3}^{i_{\max}} c_i(\mathbf{r})\zeta(i, t_{\text{fin}} + 1) \end{aligned} \tag{43}$$

where $\zeta(i,j)$ denotes the Hurwitz zeta function, a generalization of the well-known Riemann zeta function. In our approach, the sum over the infinitely many cells is therefore not truncated but approximated by the analytical sum of its parametrized asymptotic form. The advantage of this approach is that it requires only a standard Coulomb potential evaluation for a finite number of nearby cells, allowing for tests of convergence of the scheme by varying the t_{init} and t_{fin} parameters. In the following section, we extend this simple approach to two-dimensional periodic systems.

3.2.3. Topological Potential Extrapolation for Two-Dimensional Periodic Systems. For two-dimensional periodic systems, i.e., slabs, the lattice vectors will be defined as $\mathbf{R} = na_x\mathbf{i} + mb_x\mathbf{i} + mb_y\mathbf{j}$, where n and m are integer numbers, $\mathbf{i}$ and $\mathbf{j}$ represent the x- and y-axis unit vectors, and a_x, b_x, and b_y define the cell's geometry.

To extend the 1D derivation to 2D systems, we have to define a suitable topological distance t

$$t = |n| + |m| \tag{44}$$

dx.doi.org/10.1021/ct500172n | J. Chem. Theory Comput. XXXX, XXX, XXX−XXX

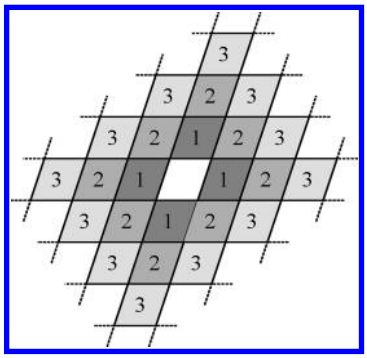

Figure 1. Schematic representation of the first few topological shells in a 2D periodic system.

For each cell that lies at a distance t from the central cell, there is always a cell with equal topological distance but opposite lattice translation.

The total Coulomb potential is thus a combination of potentials originating from different topological shells

$$V_{\text{def}}(\mathbf{r}) = \sum_{t=0}^{\infty} V_t(\mathbf{r}) \tag{45}$$

$$V_t(\mathbf{r}) = \sum_{n=-\infty}^{\infty} \sum_{m=-\infty}^{\infty} \delta(|m| + |n| - t) V_{\text{def}}^{\text{cell}}(\mathbf{r} - \mathbf{R}) \tag{46}$$

If the cells of a given topological shell are far enough from the central cell, the potential originating from each cell reduces to a multipole expansion (as in the 1D case, the potential of the orthogonal d_z dipole and of higher multipoles will decay as $1/R^3$ or faster)

$$V_t(\mathbf{r}) \propto \sum_{n=-\infty}^{\infty} \sum_{m=-\infty}^{\infty} \delta(|m| + |n| - t) \times \left(\frac{(y - mb_y)d_y}{\|\mathbf{r} - \mathbf{R}\|^3} + \frac{(x - na_x - mb_x)d_x}{\|\mathbf{r} - \mathbf{R}\|^3} + O\left(\frac{1}{\|\mathbf{r} - \mathbf{R}\|^3}\right)\right) \tag{47}$$

In the long distance limit

$$\frac{1}{\|\mathbf{r} - \mathbf{R}\|^3} = \frac{1}{\|\mathbf{R}\|^3} + O\left(\frac{1}{\|\mathbf{R}\|^4}\right) \text{ as } t \to \infty \tag{48}$$

In this limit, eq 47 simplifies to

$$V_{t\to\infty}(\mathbf{r}) \propto \sum_{n=-\infty}^{\infty} \sum_{m=-\infty}^{\infty} \delta(|m| + |n| - t) \times \left(\frac{(y - mb_y)d_y}{\|\mathbf{R}\|^3} + \frac{(x - na_x - mb_x)d_x}{\|\mathbf{R}\|^3} + O\left(\frac{1}{\|\mathbf{R}\|^3}\right)\right) \tag{49}$$

We now exploit the fact that for each cell of given topological order, there is a cell with opposite n and m in the same topological shell

$$V_{t\to\infty}(\mathbf{r}) \propto \sum_{n=0}^{\infty} \sum_{m=0}^{\infty} \delta(m + n - t) \times \left(\frac{(y - mb_y)d_y}{\|\mathbf{R}\|^3} + \frac{(x - na_x - mb_x)d_x}{\|\mathbf{R}\|^3} + \frac{(y + mb_y)d_y}{\|\mathbf{R}\|^3} + \frac{(x - na_x + mb_x)d_x}{\|\mathbf{R}\|^3} + \frac{(y - mb_y)d_y}{\|\mathbf{R}\|^3} + \frac{(x + na_x - mb_x)d_x}{\|\mathbf{R}\|^3} + \frac{(y + mb_y)d_y}{\|\mathbf{R}\|^3} + \frac{(x + na_x + mb_x)d_x}{\|\mathbf{R}\|^3} + O\left(\frac{1}{\|\mathbf{R}\|^3}\right)\right) \tag{50}$$

After simplifying, we obtain

$$V_{t\to\infty}(\mathbf{r}) \propto \sum_{n=0}^{\infty} \sum_{m=0}^{\infty} \delta(m + n - t) \times \left(\frac{4yd_y}{\|\mathbf{R}\|^3} + \frac{4xd_x}{\|\mathbf{R}\|^3} + O\left(\frac{1}{\|\mathbf{R}\|^3}\right)\right) \propto \sum_{n=0}^{\infty} \sum_{m=0}^{\infty} \delta(m + n - t) O\left(\frac{1}{\|\mathbf{R}\|^3}\right) \tag{51}$$

Making explicit use of the constraint $m + n = t$, one can express $\|\mathbf{R}\|$ as

$$\|\mathbf{R}\| = \sqrt{n^2 a_x^2 + n(t - n)a_x b_x + (t - n)^2 (b_x + b_y)^2} \tag{52}$$

Because $n \leq t$

$$\|\mathbf{R}\| = O(t) \text{ as } t \to \infty \tag{53}$$

Because of the Kronecker delta function in eq 51, the double sum reduces to a single sum from zero to t

$$V_{t\to\infty}(\mathbf{r}) = \sum_{n=0}^{t} O\left(\frac{1}{t^3}\right) \tag{54}$$

making the sum going asymptotically as $O(1/t^2)$ for large t. This limiting behavior allows us to, just like in the one-dimensional case, fit the coefficients of the large distance limit of $V_t(\mathbf{r})$. The only difference is that we now need to include as leading term $1/t^2$, alongside with higher order terms

$$V_{t\to\infty}(\mathbf{r}) = \frac{c_2(\mathbf{r})}{t^2} + \frac{c_3(\mathbf{r})}{t^3} + \ldots \tag{55}$$

We then proceed as described in 3.2.2. The coefficients $c_i(\mathbf{r})$ are fitted from $V_t(\mathbf{r})$ versus t using a finite set of t ($t_{\text{init}} \leq t \leq t_{\text{fin}}$), for which the potential $V_t(\mathbf{r})$ is calculated explicitly. With the coefficients known, the infinite sum of the long-range potential can be carried out analytically. The total Coulomb potential $V_{\text{def}}(\mathbf{r})$ can be approximated by

$$V_{\text{def}}(\mathbf{r}) \approx V_{\text{def}}^{\text{cell}}(\mathbf{r}) + \sum_{t=1}^{t_{\text{fin}}} V_t(\mathbf{r}) + \sum_{i=2}^{i_{\max}} c_i(\mathbf{r}) \zeta(i, t_{\text{fin}} + 1) \tag{56}$$

3.2.4. Charge Renormalization. Because artificial monopole contributions due to numerical noise may lead to divergencies, care should be taken in the numerical accuracy of the fit procedure for periodic systems. In the fitting procedure described in Sections 2.2 and 3.1, we did not explicitly

dx.doi.org/10.1021/ct500172n | J. Chem. Theory Comput. XXXX, XXX, XXX−XXX

Table 1. Parameters for Various Normal Settings

name	l_{margin}	c_{acc}	l_{grid}	i^{1D}_{max}	i^{2D}_{max}	t_{init}	t_{fin}	ΔE^a
default	4	3	$2l_{max} + 1$	4	3	5	11	8×10^{-3}
good	6	6	$2l_{max} + 7$	4	3	6	13	1×10^{-3}
very good	8	10	$2l_{max} + 13$	4	3	7	15	3×10^{-4}
excellent	12	14	$2l_{max} + 20$	4	3	9	19	6×10^{-5}
benchmark	16	20	$2l_{max} + 26$	4	3	14	29	

[a]Estimated bonding energy accuracy per atom in kcal/mol for organic molecules (see Section 5.2).

constrain the fitted deformation density to integrate to zero over the unit cell, and we did indeed observe a small nonzero total charge in the unit cell in actual calculations.

Because the resulting divergence is caused only by the long-range part of the Coulomb potential, it can be avoided by a simple renormalization of the monopole charges in the potential multipole expansion. The residual charge in the unit cell is

$$\Delta q_{def} = \sum_{i \in Atoms} q_i^{0,0} \tag{57}$$

so that the correct asymptotic behavior of the Coulomb potential V_{def} is enforced by a uniform shift of the monopole charges

$$\bar{q}_i^{0,0} = q_i^{0,0} - \frac{\Delta q_{def}}{N_{atoms}} \tag{58}$$

The corrected long-range Coulomb potential (eq 17) and the short-range potential (eq 16) are matched at a switching radius r^{max} to ensures continuity of the potential and its first first derivative. This simple pragmatic approach remedies the residual charge issue without introducing the complication of requiring a charge constraint during the fitting procedure.

4. TECHNICAL DETAILS

In establishing a well-balanced set of default parameters, formal arguments need to be combined with a good deal of empiricism to find the best compromises between accuracy and efficiency. In this section, we describe the ideas behind our implementational choices as well as the definition of five default parameter sets. As mentioned in Section 2.2, one of the critical aspects of the scheme is the convergence of the angular and radial expansion in eq 8. The partitioned density $\rho_i(\mathbf{r})$ contains contributions from basis functions centered on atoms other than i. Because the spherical harmonic expansion of a spherical harmonic on a different center is an infinite series, the expansion of eq 8 is formally only exact for $l_{max} = \infty$. Despite this, thanks to the smooth shape of the space partition function, the expansion length in eq 8 can in practice be truncated to a finite l_{max}. As a function of this tunable parameter, the polar expansion error monotonously converges to zero. We thereby empirically relate the expansion order l_{max} to the maximum l-value present in the basis set l^{basis}_{max} and use as a prescription

$$l_{max} = \max(2 \times l^{basis}_{max}, l_{margin} + l^{basis}_{max}) \tag{59}$$

where l_{margin} is an "accuracy"-dependent parameter. The order of the Lebedev polar grids l_{grid} employed in the numerical evaluation of the integral in eq 9 is then also chosen as a function of this l_{max} as specified in Table 1.

Besides making a choice for the angular integration truncation parameters, we also need a criterion to decide on the number of radial interpolation points. As in a previous work,[26] we first define n_i^0 as the minimum number of radial integration points needed to integrate the norm of all basis functions on the atom i with a relative error smaller than 5×10^{-6}. We next introduce a simple scaling algorithm to adjust the number of radial interpolation points per atom type n_i^{rad} (the index i labels the atom types) to reach a desired accuracy

$$n_i^{rad} = n_i^0 \times c_{acc} \tag{60}$$

In Table 1, we list the parameters of four default settings and the respective expected density and energy accuracy, relative to the benchmark settings. The topological extrapolation of the long-range Coulomb potential described in Section 3.2 has three parameters: i_{max}, t_{fin}, and t_{init}. Their values for different settings are also listed in Table 1.

The applicability of the fitting scheme described in the present work is not restricted to calculation of the Coulomb potential of electron densities. Other (often more numerically delicate) quantities can be fitted with this scheme, such as density nuclear derivatives used in the computation of analytical second derivatives, and the transition densities used in time-dependent DFT.

5. BENCHMARK CALCULATIONS AND DISCUSSION

In this section, we present benchmark studies of molecular and periodic systems. Unless otherwise indicated, in all the calculations discussed in the following sections, the TZP basis set[37] was used alongside with the Becke–Perdew[38,39] exchange-correlation functional (BP86) and the scalar relativistic ZORA Hamiltonian.[40] Calculations of periodic systems have been performed with the program BAND[12] (in which an alternative global auxiliary fit set method combined with screening was already implemented), while for molecules, we used the program ADF[21] (in which an alternative pair-based auxiliary fit set method[8] was already implemented).

5.1. Asserting the Topological Extrapolation of the Coulomb Potential. The slow convergence of a direct lattice summation of the Coulomb potential discussed in Section 3.2 is clearly visible in Figures 2 and 3, in which the formation energy of a Molybdenum-disulfide nanotube and slab for different truncations of the lattice sum of eq 30 are shown. In order to obtain a milli-eV formation energy accuracy for the two test systems, a huge number of cells has to be taken into account: several hundred for the one-dimensional system and almost one million for the two-dimensional system (Figure 4).

By extrapolating the long-range Coulomb potential contribution as described in Sections 3.2.3 and 3.2.2, the error in the formation energy drops in the sub-milli-eV region with less than 10 topological shells and to the sub-0.1-milli-eV domain with less than 20 shells, as shown in Figures 2 and 3. The data points relative to the extrapolated long-range Coulomb potential in Figures 2 and 3 correspond to the four settings listed in Table 1.

dx.doi.org/10.1021/ct500172n | J. Chem. Theory Comput. XXXX, XXX, XXX–XXX

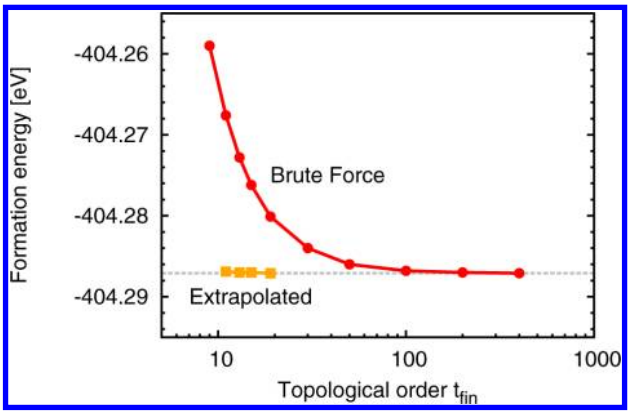

Figure 2. Formation energy of a (11,0) MoS_2 nanotube (1D).

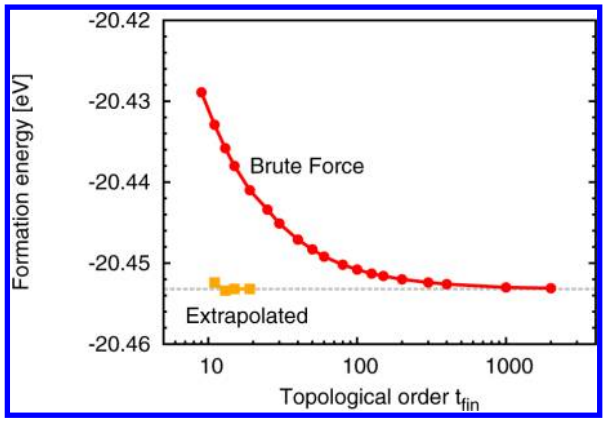

Figure 3. Formation energy of a MoS_2 monolayer (2D).

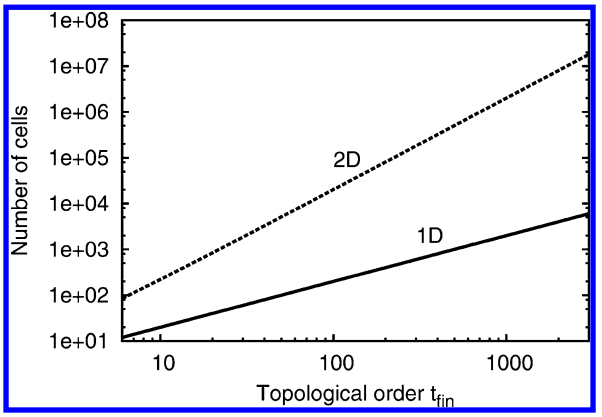

Figure 4. Total number of cells of topological order $t \leq t_{fin}$ as a function of t_{fin}.

One could in principle combine the FMM technique[41] with our scheme to efficiently increase the value of t_{fin}, which determines the amount of cells evaluated explicitly. In our experience thus far, this was not necessary as the topological extrapolation of the long-range potential is usually not very time consuming (this is discussed in detail in Section 5.4).

5.2. Absolute Accuracy of the Scheme. The quality of the fitted density can be directly tested; to this end, we define $\Delta\rho$ as $\Delta\rho = 1/n_e(\int(\rho(\mathbf{r})) - \rho_{fit}(\mathbf{r}))^2 d\mathbf{r})^{1/2}$, where n_e is the number of electrons (not including the frozen core).[37] This quantity is of course not trivially related to the error in the Coulomb potential. In absence of an exact analytical expression of the Coulomb potential for STOs and NAOs, the accuracy of the method can only be validated through internal consistency, comparison to different fitting schemes, or by indirect measures.

Various classes of systems will be used to benchmark our fitting scheme: organic molecules (Baker test set,[42] consisting of 30 organic molecules of small and medium size), group six metal hexacarbonyls, and a set of transition metal dichalcogenides crystals and slabs. Tables 2 and 3 collect the root-mean-square errors (RMSE) of various quantities of interest for the different test-sets. The "benchmark" settings, defined in Table 1, have been used to calculate the reference values. For all the investigated properties, our fitting scheme (with "excellent" settings) appears to be at least 1 order of magnitude more accurate than the most accurate of the auxiliary basis set methods tested.

A major advantage of our method over the auxiliary basis set method is how easily high accuracy can be achieved. Once the density is partitioned into atom-centered contributions (which we remind is an exact procedure), the fully numerical expansion of eq 12 has virtually no accuracy limitation. Using spatially extended auxiliary radial function, as opposed to our local radial projections, introduces basis-set linear dependency as a subtle accuracy-limiting factor.[43,44] Beyond a certain point, the linear dependency of the auxiliary functions will lead to numerical instability and adding functions will not improve the accuracy anymore. Designing fit sets is therefore a delicate task, and various procedures effectively aimed to minimize the linear dependency problem have been proposed.[14,45] The severeness of this linear dependency problem also depends on the particular fitting procedure employed, e.g., a global fit procedure is more harshly afflicted by linear dependency issues than a pair-based fit procedure (which, however, has other drawbacks[10]). For the ADF pair fit implementation, we note that the QZ4P fit set is the largest fit set available for routine usage[37] because adding extra functions leads to numerical instabilities.

5.3. U_2H_2. The implementation in the program ADF of the pair-based fitting described in ref 8 cannot deal with fit functions of angular momentum l larger than 4. Although this is merely a technical issue and not an intrinsic limitation of the scheme itself, it is in practice a rather severe problem when dealing with particular compounds containing elements of the *f*-block. For specific electronic configurations or bonding situations involving *f*-block elements, the one-center part of the density can have an *h*-like character, intrinsically unrepresentable by a linear combination of fit functions with $l \leq 4$.

An example of such a system is the rhombic (hydrogen-bridged) configuration of the U_2H_2 molecule. The error in the bonding energy due to the lack of high angular momentum fit-functions ($l > 4$) is as large as 0.1 eV, roughly 3 kcal/mol. Using our scheme, the error due to fit inaccuracies can be as small as few micro-eV. Although not all compounds containing *f*-block elements present this problem, the lack of high angular momentum fit functions represents a serious practical limitation of the above-mentioned implementation.

5.4. Scaling and Performance. First, the expansion procedure described in Section 2.2 requires the evaluation of the partitioned electron densities $\rho_i(\mathbf{r})$ on the fitting grid. For this step, we use standard linear scaling density evaluation techniques, as implemented in ADF and BAND.[21] Next, the evaluation of the fitted density and density derivatives (needed for the XC potential) for a given integration point formally

dx.doi.org/10.1021/ct500172n | J. Chem. Theory Comput. XXXX, XXX, XXX−XXX

Table 2. Comparison of Different Fitting Schemes for Molecular Systems

	organic molecules (Baker Set)					Cr/Mo/W hexacarbonyls				
name	ΔE^a	$\Delta\varepsilon^b$	$\Delta\omega^c$	$\Delta\nu^d$	$\Delta\rho$ [10^{-3}]	ΔE^a	$\Delta\varepsilon^b$	$\Delta\omega^c$	$\Delta\nu^d$	$\Delta\rho$ [10^{-3}]
normal	0.3	5	6	3	5	0.5	3	8	0.8	5
good	0.05	2	2	0.5	2	0.09	3	5	0.3	2
very good	0.01	0.4	0.4	0.2	0.7	0.01	2	2	0.2	0.8
excellent	0.002	0.2	0.1	0.07	0.1	0.0006	0.3	0.4	0.04	0.2
	auxiliary basis-set method (pair-based)									
normal[e]	1	40	50	3	2	0.6	7	11	2	4
QZ4P[e]	0.04	6	8	0.9	0.9	0.03	4	5	0.7	0.6

[a]Bonding energy per atom RMSE in milli-eV. [b]Kohn−Sham HOMO−LUMO energy difference RMSE in milli-eV. [c]Time-dependent DFT lowest singlet−singlet excitation energy RMSE in milli-eV. [d]Analytical infrared frequencies RMSE in cm^{-1}. [e]"Default" and "QZ4P" refer to two auxiliary fit sets described in ref 37.

Table 3. Comparison of Different Fitting Schemes for Transition Metal Dichalcogenides Crystals and Slabs: MQ_2 (M = V, Cr, Nb, Mo, Ta, W; Q = S, Se, Te)

	crystals			slabs		
name	ΔE^a	$\Delta\varepsilon^b$	$\Delta\rho$ [10^{-3}]	ΔE^a	$\Delta\varepsilon^b$	$\Delta\rho$ [10^{-3}]
normal	0.5	1.0	0.1	1.0	1.5	0.3
good	0.3	0.8	0.08	0.6	0.6	0.1
very good	0.2	1.0	0.04	0.4	1.0	0.09
excellent	0.06	0.2	0.02	0.1	0.5	0.05
	auxiliary basis-set method (global)					
normal[c]	2.0	4.0	0.4	3.0	3.0	0.6

[a]Bonding energy per atom RMSE in milli-eV. [b]Kohn−Sham HOMO−LUMO energy difference RMSE in milli-eV. [c]"Default" refers to the auxiliary fit set described in ref 37.

scales linearly with the number of atoms; therefore, the evaluation of these quantities on the full integration grid formally scales quadratically. However, because of the localized nature of the partitioned densities $\rho_i(\mathbf{r})$, it is straightforward to introduce distance cutoffs to make the evaluation of these quantities linear scaling. Finally, the evaluation of the potential has a formal quadratic scaling, which again can be brought down to linear scaling by using distance cut-offs. The only exception is the multipole potential (see Section 2.4), for which the cutoff distance needs to be extremely large, making this part scale quadratically in practice. This evaluation does, however, have a small prefactor. If this step does become important in the future, one may combine the current scheme with the FMM to reduce it to linear computational scaling as well.

In Table 4, we summarize the most important operations discussed in the work for which we will show the practical performance. The other major steps that are important in assessing the efficiency of the DFT program are the evaluation of the Fock matrix elements (numerical integration of the product of basis functions and potential) and the diagonalization of the Fock matrix to obtain the Kohn−Sham orbitals. For the first of these steps, reduced scaling techniques are also currently employed. Detailed discussion of the efficiency of these steps falls outside the scope of this paper (see ref 46 for a recent review), but we will list some representative overall timings of an Self-Consistent Field (SCF) step to put the fit-related work into perspective. All simulations presented in this section were performed on a 2.60 GHz 16 cores Intel Xeon (E5−2650v2) CPU with 64 GB of RAM.

Table 4. Summary of the Most Important Steps of the Density Fitting Procedure

1. Expansion	(1.a) Evaluation of $\rho_i(\mathbf{r})$ on the fitting grid	eqs 4 and 25
	(1.b) Projection onto spherical harmonics	eq 9
	(1.c) Evaluation of the spline coefficients	eq 10
2. Density and derivatives	(2.a) Fitted density on the integration grid	eq 12
	(2.b) Fitted density gradients and second derivatives on the integration grid	
3. Potential evaluation	(3.a) Radial Coulomb integrals	eq 15
	(3.b) Short range potential	eqs 16 and 17
	(3.c) Multipole potential	eq 17
	(3.d) Long range potential (periodic)	eqs 34, 42, and 55

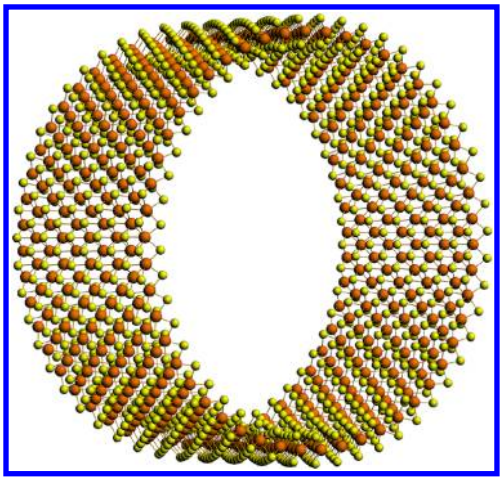

Figure 5. ZigZag-50 MoS_2 nanotube (5 unit cells repetitions are shown).

5.4.1. Molybdenum-Disulfide Periodic Systems. In Table 5, we show the timings for a single SCF step for various MoS_2 systems.[47] The calculations were performed using the periodic DFT code BAND with "normal" fit settings and intentionally disregarding point group symmetry. To simplify comparisons, we kept the k-space sampling independent of the system size, using 3 and 9 k-points for 1D and 2D systems, respectively. Note that for the larger 2D systems this arguably constitutes an oversampling of the reciprocal space.

The "total fit" timings in Table 5 contain all the fitting steps described in Table 4; only a relatively small fraction of the total elapsed time is spent in fit related operations. For MoS_2 slabs, the relative impact of the fitting procedure to the total SCF step decreases with system size. The timings are clearly dominated

dx.doi.org/10.1021/ct500172n | J. Chem. Theory Comput. XXXX, XXX, XXX−XXX

Table 5. Elapsed Time per SCF Step (in seconds) Spent on Fitting Related Operations (with "default" fit settings) for Various MoS_2 Systems[a]

				expansion			density and deriviatives		potential evaluation				global fit[b]	
system	# atoms	SCF step (total)	total fit (per step)	1.a	1.b	1.c	2.a	2.b	3.a	3.b	3.c	3.d	prep.[c]	fit[d]
MoS_2 slab (supercells)														
1 × 1	3	0.4	0.19	0.03	< 0.01	< 0.01	0.02	0.06	0.01	0.02	0.01	0.05	0.3	0.6
2 × 2	12	2.1	0.98	0.2	0.01	< 0.01	0.07	0.3	0.01	0.10	0.11	0.18	3.4	3.5
3 × 3	27	9.3	2.8	1.2	0.02	< 0.01	0.14	0.5	0.01	0.25	0.29	0.4	16.5	9.6
4 × 4	48	31.8	8.9	5.6	0.02	< 0.01	0.3	0.9	0.01	0.6	0.8	0.7	56.1	21.1
5 × 5	75	79.6	17.5	11.8	0.03	0.01	0.4	1.3	0.02	1.2	1.7	1.1	150.0	36.9
MoS_2 nanotubes														
ZigZag-20	120	91.4	21.9	12.4	0.2	0.01	1.0	2.6	0.1	2.0	3.4	0.3	393.8	93.5
ZigZag-30	180	168.2	40.9	21.0	0.3	0.01	1.8	3.8	0.1	4.9	8.6	0.4	n.a.	n.a.
ZigZag-40	240	296.5	71.9	35.9	0.4	0.02	2.9	5.1	0.2	10.3	16.7	0.4	n.a.	n.a.
ZigZag-50	300	492.5	105.3	58.7	0.6	0.02	4.6	6.5	0.2	17.7	26.1	0.4	n.a.	n.a.

[a]See Table 4 for a description of the various steps. [b]"Global fit" refers to the global auxiliary fit set method already implemented in BAND.[12] [c]This is the (cubically scaling) precalculation step. [d]Elapsed time per SCF step of fitting related operations.

Table 6. Elapsed Time per SCF Step (in seconds) Spent on Fitting Related Operations for Chlorophyll-a (137 atoms) Employing Different Settings[a]

		expansion			density and deriviatives		potential evaluation			
name	total fit	1.a	1.b	1.c	2.a	2.b	3.a	3.b	3.c	3.d
normal	3.7	1.1	0.05	0.01	0.4	1.5	0.07	0.5	0.1	–
good	10.8	5.0	0.2	0.03	0.7	3.7	0.17	0.7	0.3	–
very good	36.5	23.5	1.2	0.1	2.1	7.0	0.5	1.9	0.2	–
excellent	113.6	82.0	7.5	0.3	2.7	15.7	1.6	3.7	0.1	–

[a]See Table 4 for a description of the various steps.

by step 1.a, namely, the evaluation of the partitioned densities on the fitting grid. Unlike in the MoS_2 slabs series, the multipole potential evaluation (step 3.c) constitutes a significant contribution to the total fit timing of the MoS_2 nanotubes. This is due to the large ratio between the lattice constant and the ring diameter; for this particular geometry, a large number of atomic multipoles have to be treated explicitly and cannot be combined into cellular contributions (see Section 3.2.2).

The last two columns of Table 5 contain timings of the old global auxiliary fit set method of BAND.[12] The new method has much better scaling behavior, as the global fit requires a cubically scaling inversion of the overlap matrix.[12] For all tested systems, the new method is faster; as an example, the total fit speed-up per SCF step for the MoS_2 ZigZag-20 nanotube is more than a factor four (21.9 vs 93.5 s). The precalculation step of the auxiliary fit set scheme of BAND accounts for an additional 393 s in preparation to the SCF procedure. Furthermore, because of the high memory usage of the global auxiliary fit set method, the larger nanotubes presented in Table 5 (ZigZag-30, -40, and -50) cannot be calculated on our benchmark computer with 64 GB of RAM.

5.4.2. Chlorophyll-a. In Table 6, we compare timings for Chlorophyll-a employing different fit settings, as defined in Table 1. These calculations were performed using the molecular DFT code ADF. Using the new "normal" settings, which yields a level of accuracy sufficient for most standard applications, the computational burden of all fitting related operations is comparable to the rest of the SCF step (approximately 3 s). If higher accuracy is needed, more precise settings can be used; in the case of "excellent" setting, the fitting is almost 30 times more expensive than "normal" (mainly due to step 1.a) but can be up to 2 orders of magnitude more accurate.

Using the pair-based auxiliary fit set method already implemented in ADF,[21] the elapsed time per SCF step spent on fitting related operations is 1.4 and 2.2 s using the old "default" and the more precise "QZ4P" fit set, respectively.[37]P-Prior to the SCF procedure, certain overlap integrals have to be precalculated, accounting for an additional 4.7 and 14.5 s, respectively. For this particular example, SCF convergence was achieved in 31 steps using the "default" fit set, while only 20 steps were necessary employing "QZ4P" fit set. Employing our new "normal" method, SCF convergency was likewise achieved in 20 steps. Altogether, the total elapsed time spent on fitting related operations for the full SCF procedure is 48.1 and 58.5 s for the "default" and "QZ4P" pair-based auxiliary fit set methods, respectively, and 76.7 s for our "normal" method. In practice, we noted that the use of a more accurate fitting, thus increasing the time per SCF step, can sometimes speed up the overall calculation, as the improved numerical precision (and thereby reduced numerical noise) leads to a faster convergence of iterative procedures such as self-consistent fields and geometry optimizations. This allows for further fine-tuning of the parameters for specific purposes, which we plan to explore in a subsequent work.

6. CONCLUSIONS

In this paper, we have described an efficient and nearly linear scaling implementation of a basis set independent numerical density fitting scheme in which periodic and nonperiodic systems are treated on an equal footing. Virtually arbitrary accuracy can be achieved for various molecular and crystalline properties, while this level of accuracy is difficult to achieve with

dx.doi.org/10.1021/ct500172n | J. Chem. Theory Comput. XXXX, XXX, XXX−XXX

auxiliary basis set fit methods. Furthermore, we introduced a simple and efficient approach for the evaluation of long-range Coulomb potential contribution in 1D and 2D periodic systems.

■ ASSOCIATED CONTENT

Supporting Information

Information as mentioned in the text. This material is available free of charge via the Internet at http://pubs.acs.org.

■ AUTHOR INFORMATION

Corresponding Author

*E-mail: l.visscher@vu.nl.

Notes

The authors declare no competing financial interest.

■ REFERENCES

(1) Eichkorn, K.; Treutler, O.; Öhm, H.; Häser, M.; Ahlrichs, R. *Chem. Phys. Lett.* **1995**, *240*, 283−290.
(2) VandeVondele, J.; Krack, M.; Mohamed, F.; Parrinello, M.; Chassaing, T.; Hutter, J. *Comput. Phys. Commun.* **2005**, *167*, 103−128.
(3) Kantorovich, L. *Quantum Theory of the Solid State: An Introduction*; Kluwer Academic Publishers: Dordrecht, The Netherlands, 2004; pp 88−99.
(4) Neugebauer, J.; Scheffler, M. *Phys. Rev. B* **1992**, *46*, 16067−16080.
(5) Füsti-Molnár, L.; Pulay, P. *J. Chem. Phys.* **2002**, *117*, 7827−7835.
(6) Jarvis, M. R.; White, I. D.; Godby, R. W.; Payne, M. C. *Phys. Rev. B* **1997**, *56*, 14972−14978.
(7) Yu, L.; Ranjan, V.; Lu, W.; Bernholc, J.; Nardelli, M. B. *Phys. Rev. B* **2008**, *77*, 245102.
(8) Baerends, E.; Ellis, D.; Ros, P. *Chem. Phys.* **1973**, *2*, 41−51.
(9) Burow, A. M.; Sierka, M.; Mohamed, F. *J. Chem. Phys.* **2009**, *131*, 214101.
(10) Merlot, P.; Kjaergaard, T.; Helgaker, T.; Lindh, R.; Aquilante, F.; Reine, S.; Pedersen, T. B. *J. Comput. Chem.* **2013**, *34*, 1486−1496.
(11) Ren, X.; Rinke, P.; Blum, V.; Wieferink, J.; Tkatchenko, A.; Sanfilippo, A.; Reuter, K.; Scheffler, M. *New J. Phys.* **2012**, *14*, 053020.
(12) te Velde, G.; Baerends, E. J. *Phys. Rev. B* **1991**, *44*, 7888−7903.
(13) Jaffe, J. E.; Hess, A. C. *J. Chem. Phys.* **1996**, *105*, 10983−10998.
(14) Aquilante, F.; Gagliardi, L.; Pedersen, T. B.; Lindh, R. *J. Chem. Phys.* **2009**, *130*, 154107.
(15) Aquilante, F.; Lindh, R.; Pedersen, T. B. *J. Chem. Phys.* **2007**, *127*, 114107.
(16) Becke, A. D.; Dickson, R. M. *J. Chem. Phys.* **1988**, *89*, 2993.
(17) Delley, B. *J. Chem. Phys.* **1990**, *92*, 508−517.
(18) Delley, B. *J. Phys. Chem.* **1996**, *100*, 6107−6110.
(19) Lopez, R.; Ramirez, G.; Ema, I.; Rico, J. F. *J. Comput. Chem.* **2013**, *34*, 1800−1809.
(20) Termath, V.; Handy, N. C. *Chem. Phys. Lett.* **1994**, *230*, 17−24.
(21) te Velde, G.; Bickelhaupt, F. M.; Baerends, E. J.; Fonseca Guerra, C.; van Gisbergen, S. J. A.; Snijders, J. G.; Ziegler, T. *J. Comput. Chem.* **2001**, *22*, 931−967.
(22) Becke, A. D. *J. Chem. Phys.* **1988**, *88*, 2547.
(23) Stratmann, R.; Scuseria, G. E.; Frisch, M. J. *Chem. Phys. Lett.* **1996**, *257*, 213−223.
(24) Pérez-Jorda, J.; Yang, W. *Chem. Phys. Lett.* **1995**, *241*, 469−476.
(25) Boys, S.; Rajagopal, P. *Adv. Quantum Chem.* **1966**, *2*, 1−24.
(26) Franchini, M.; Philipsen, P. H. T.; Visscher, L. *J. Comput. Chem.* **2013**, *34*, 1819−1827.
(27) Treutler, O.; Ahlrichs, R. *J. Chem. Phys.* **1995**, *102*, 346−354.
(28) Lebedev, V. I.; Laikov, D. N. *Dokl. Math.* **1999**, *59* (3), 477−481.
(29) Press, W. H.; Flannery, B. P.; Teukolsky, S. A.; Vetterling, W. T. *Numerical Recipes in C: The Art of Scientific Computing*, Second ed.; Cambridge University Press: Cambridge, U.K., 1992; p 113.
(30) Jackson, J. *Classical Electrodynamics*; Springer: 2004; p 136.
(31) Takemoto, H.; Ohyama, T.; Tohsaki, A. *Prog. Theor. Phys.* **2003**, *109*, 563−573.
(32) Ewald, P. P. *Ann. Phys.* **1921**, *369*, 253−287.
(33) Lambert, C. G.; Darden, T. A., Jr.; J. A. B. *J. Comput. Phys.* **1996**, *126*, 274−285.
(34) Kudin, K. N.; Scuseria, G. E. *Phys. Rev. B* **2000**, *61*, 16440−16453.
(35) Lindbo, D.; Tornberg, A.-K. *J. Chem. Phys.* **2012**, *136*, 164111.
(36) D'Urso, C.; Adelberger, E. G. *Phys. Rev. D* **1997**, *55*, 7970−7972.
(37) van Lenthe, E.; Baerends, E. J. *J. Comput. Chem.* **2003**, *24*, 1142−1156.
(38) Becke, A. D. *Phys. Rev. A* **1988**, *38*, 3098−3100.
(39) Perdew, J. P. *Phys. Rev. B* **1986**, *33*, 8822−8824.
(40) van Lenthe, E.; Baerends, E. J.; Snijders, J. G. *J. Chem. Phys.* **1993**, *99*, 4597−4610.
(41) Greengard, L.; Rokhlin, V. *J. Comput. Phys.* **1987**, *73*, 325−348.
(42) Baker, J.; Kessi, A.; Delley, B. *J. Chem. Phys.* **1996**, *105* (1), 192−212.
(43) Sodt, A.; Subotnik, J. E.; Head-Gordon, M. *J. Chem. Phys.* **2006**, *125*, 194109.
(44) Kobko, N.; Dannenberg, J. J. *J. Phys. Chem. A* **2001**, *105*, 1944−1950.
(45) Foerster, D. *J. Chem. Phys.* **2008**, *128*, 034108.
(46) Bowler, D. R.; Miyazaki, T. *Rep. Prog. Phys.* **2012**, *75*, 036503.
(47) Zibouche, N.; Kuc, A.; Heine, T. *Eur. Phys. J. B* **2012**, *85*, 1−7.